ACS APPLIED MATERIALS & INTERFACES

Biological and Medical Applications of Materials and Interfaces

Iodine-rich polymersomes enable versatile SPECT/CT imaging and potent radioisotope therapy for tumor in vivo

Jinsong Cao, Yaohua Wei, Yanxiang Zhang, Guanglin Wang, Xiang Ji, and Zhiyuan Zhong

ACS Appl. Mater. Interfaces, **Just Accepted Manuscript** • DOI: 10.1021/acsami.9b04294 • Publication Date (Web): 07 May 2019

Just Accepted

ACS Publications

is published by the American Chemical Society. 1155 Sixteenth Street N.W., Washington, DC 20036

Iodine-rich Polymersomes Enable Versatile SPECT/CT Imaging and Potent Radioisotope Therapy for Tumor In Vivo

Jinsong Cao[1, 2], Yaohua Wei[1], Yanxiang Zhang[2], Guanglin Wang[2*], Xiang Ji[3], Zhiyuan Zhong[1*]

[1]Biomedical Polymers Laboratory, College of Chemistry Chemical Engineering and Materials Science, and State Key Laboratory of Radiation Medicine and Protection, Soochow University, Suzhou 215123, PR China

[2]State Key Laboratory of Radiation Medicine and Protection, School of Radiation Medicine and Protection & School for Radiological and Interdisciplinary Sciences (RAD-X), Collaborative Innovation Center of Radiation Medicine of Jiangsu Higher Education Institutions, Soochow University, Suzhou 215123, PR China.

[3]Institute of Nuclear Energy Safety Technology, Chinese Academy of Sciences, Hefei 230031, PR China

Abstract

Emerging tumor treatment demands on high-sensitivity and high-spatial resolution diagnosis in combination with targeted therapy. Here, we report that iodine-rich polymersomes (I-PS) enable versatile SPECT/CT dual modal imaging and potent radioisotope therapy of breast cancer in vivo. Interestingly, I-PS could be easily and stably labeled with radioiodine, ^{125}I and ^{131}I. Dynamic light scattering and transmission electron microscopy showed that ^{125}I-PS had a size of 106 nm and vesicular morphology, similar to the parent I-PS. MTT assays displayed that I-PS and ^{125}I-PS were non-cytotoxic while ^{131}I-PS caused significant death of 4T1 cells at 5 mg PS/mL with radioactivity 12 μCi. Pharmacokinetic and biodistribution studies showed that ^{125}I-PS have a prolonged circulation and distribute mainly in tumor and reticuloendothelial system. The intravenous injection of ^{125}I-PS to 4T1 murine breast tumor-bearing mice allowed simultaneous high sensitivity and high-spatial resolution imaging of tumor by SPECT and CT, respectively. The therapeutic studies revealed that ^{131}I-PS could effectively retard growth of 4T1 breast tumor and significantly prolong mice survival time. H&E staining assay proved that ^{131}I-PS induced tumor cell death. I-PS emerges as a robust and versatile platform for dual modal imaging and targeted radioisotope therapy.

Keywords: Polymersomes; Contrast Agents; SPECT/CT; Theranostics; Radioisotope

Introduction

Relying on the high-sensitivity and high-spatial resolution diagnosis, combined therapy has attracted great attention in recent years.[1,2] Single photon emission computed tomography (SPECT) with a high sensitivity and functional imaging is widely used for cancer theranostics.[3] Owing to the limitation of the anatomical information of SPECT imaging, X-ray computed tomography (CT) has been widely conducted for patients imaging due to its high spatial and density resolution and provides the information of anatomic structure.[4,5] However, compared to SPECT imaging, CT imaging lacks sufficient sensitivity and molecular information. To overcome the limitations of single modal imaging, dual and multi-modal imaging has attracted great attention.[6-10] For instance, ^{99m}Tc-labeled dendrimer-entrapped gold nanoparticles,[11-14,] ^{99m}Tc-labeled dendrimer with iodine[15] and ^{153}Sm-labeled lanthanide-based nanoparticles[16,17] have recently been designed and investigated for in vivo SPECT/CT imaging. These reported nano-contrast agents exhibited significant improvements of both SPECT and CT signals in tumor, sentinel lymph node and atherosclerosis plaques. However, huge dose of CT contrast agents is needed for improving the imaging sensitivity. On the other hand, given the potential toxicity, it is very difficult to translate inorganic CT contrast agents to the clinical applications. It is impendent to develop multifunctional contrast agents for multimodal imaging.

Theranostics that combines diagnostics and therapy, has received widespread interests as future personalized medicine.[18-24] Polymersomes with a vesicular structure as for liposomes are able to deliver hydrophilic and hydrophobic imaging agents and drugs, offering a versatile platform for theranostics. Compared to liposomes, polymersomes are more stable and easier to fabricate with tunable properties.[25-29] Notably, nano-sized polymersomes can target to tumor through the enhanced permeation retention (EPR) effect ("passive targeting").[30,31] Various imaging agents such as fluorescent dye, magnetic particles, quantum dots and

radionuclides have been integrated with polymersomes.[32-38] Polymersomes have also been employed for loading different drugs, including chemotherapeutics, proteins, and siRNA, for cancer treatment.[39-42] Drugs loaded in polymersomes exhibited enhanced tumor accumulation and significantly improved anticancer efficacy. Notably, integration of polymersomes with radionuclides labeling for radioisotope therapy has not yet been reported to our knowledge.

In the past years, different iodine-rich polymers and nanoparticles have been developed for CT imaging in that they provide several advantages over small molecule contrast agents like preventing fast renal excretion, reducing iodine hypersensitivity, prolonging circulation time, and achieving targeted imaging.[43-47] In our recent work, we have reported that iodine-rich-nanopolymersomes (I-PS) have shown great X-ray attenuation ability.[48] Compared with the Iohexol, a commercial X-ray contrast agent, I-PS possesses strong CT signals in the blood pool, reticuloendothelial system (RES) and several malignant tumors of mice after intravenous injection. In this work, we further develop I-PS as multimodal contrast agent for versatile SPECT/CT imaging and potent radioisotope therapy of tumor in vivo (Scheme 1). ^{131}I has been used for radioisotope therapy as it emits high energy beta particles that can cause cell DNA strand breaks and induce cell death, while ^{125}I is mostly used for imaging as it emits Auger electron that can cause DNA strand breaks only when close to the cell nucleus.[49-51] With the radiolabeling, ^{125}I and ^{131}I labeled I-PS, were able to achieve high-efficiency CT imaging and SPECT imaging, as well as radioisotope therapy for tumors. This represents a first report on radiolabeled polymersomes for dual modal imaging guided radioisotope therapy.

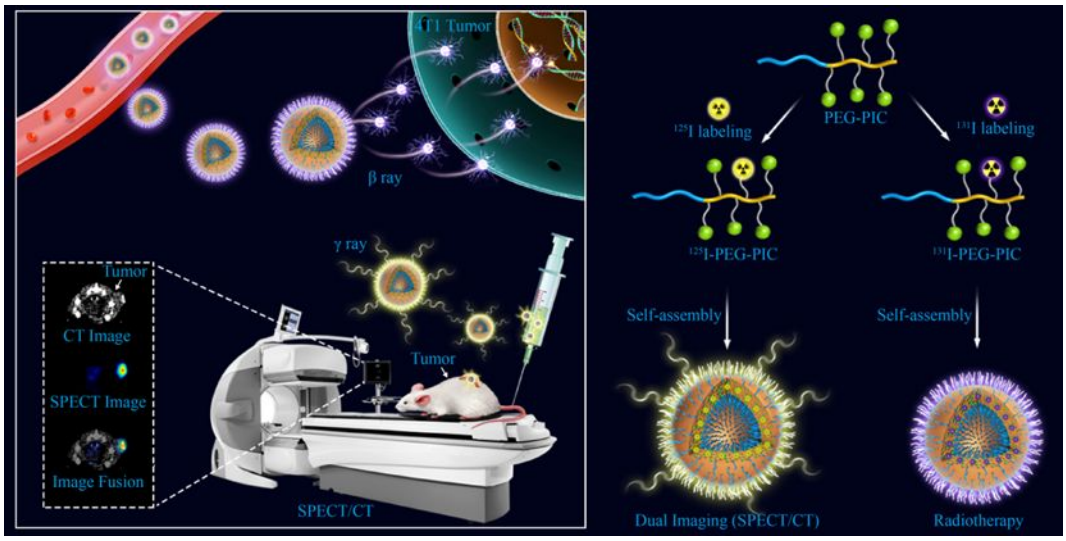

Scheme 1. A schematic illustration shows the preparation of radiolabeled iodine-rich polymersomes, ^{125}I-PS and ^{131}I-PS. ^{125}I-PS for SPECT/CT dual mode imaging and ^{131}I-PS for radioisotope therapy of cancer. PEG-PIC is an abbreviation of poly(ethylene glycol)-b-poly(iodinated carbonate) copolymer.

Materials and Method

Chemicals

Radioiodine (Na^{125}I and Na ^{131}I) was supplied by Shanghai GMS Pharmaceutical Co., Ltd. Acetic acid, dimethylformamide and ethanol were bought from Sinopharm Chemical Reagent Co., Ltd. All chemicals and reagents were used as received.

Synthesis of PEG-PIC (^{125}I) and PEG-PIC (^{131}I)

Poly(ethylene glycol)-b-poly(iodinated carbonate) (PEG-PIC) with an M_n of 5.0-50.0 kg mol^{-1} was synthesized as previously reported.[48] For synthesis of PEG-PIC (^{125}I), Na^{125}I (500 μCi, 370 mCi/mL) was mixed with ethanol (270 μL) and evaporated at 85 ºC by Thermo Shaker. PEG-PIC (1 mg) and acetic acid (2 μL) in DMF (200 μL) was added to the dry Na^{125}I (iodine in PEG-PIC/Na^{125}I molar ratio = 2.08×10^3) and heated to 70 ºC with varied time from 1 h to 10 h under shaking. Radiochemical yield was measured by thin layer chromatography assay

using saline as a mobile phase. Rf of ^{125}I-PS~0.1, Rf of free ^{125}I~0.9. PEG-PIC (^{131}I) was obtained by the same method.

Preparation of ^{125}I-PS and ^{131}I-PS

^{125}I-PS and ^{131}I-PS were prepared by solvent exchange method. In a typical example, 200 μL of PEG-PIC(^{125}I) solution in DMF (5 mg/mL) was added dropwise to 800 μL of deionized water. To remove free Na^{125}I and DMF, the resulting ^{125}I-PS dispersion was dialyzed against 200 mL of deionized water for 8 h with three times change of deionized water (MWCO = 8000 Da) and concentrated by ultrafiltration (Millipore, MWCO =10 kDa) at the speed of 4500 r/min for 10 min. ^{131}I-PS and I-PS were obtained using the same method.

The hydrodynamic radius of I-PS and ^{125}I-PS was measured by dynamic light scattering (DLS). All experiments were performed on a Malvern Zetasizer Nano ZS90 equipped with a solid-state He–Ne laser (λ = 633 nm) in triplicate at 25 ºC. Transmission electron microscope (TEM) (FEI Tecnai F20) was used to measure the size and morphology of ^{125}I-PS, manipulating at 120 kV. ^{125}I-PS (10 μL 1 mg/mL) was dropped onto a carbon coated copper grid of 200 mesh and redundant liquid was removed using a filter paper after five minutes. Phosphotungstic acid aqueous solution (10 mg/mL, 10 μL) was dropped onto copper grid to dye the ^{125}I-PS.

Cytotoxicity Assay of ^{125}I-PS and ^{131}I-PS

MTT assays were used to evaluate the cytotoxicity of ^{125}I-PS and ^{131}I-PS. 4T1 cells were seeded and cultured in 96-well plate (1×10^4 cells/well) in DMEM with 10 % fetal bovine serum (FBS) at 37 ºC for 24 h in a 5% CO_2 atmosphere. The medium was aspirated and replaced by I-PS, ^{125}I-PS and ^{131}I-PS with different concentrations (0.31, 0.63, 1.25, 2.5, 5 mg/mL, corresponding to radioactivity of 0.75, 1.5, 3, 6, 12 μCi/mL, respectively) at 37 ºC for

24 h. The cells were cultured with 3-(4,5-dimethylthiazol-2-yl)-2,5-diphenyltetrazolium bromide solution (100 μl, 0.5 mg/mL) for 4 h before the addition of dimethyl sulfoxide (100 μL). A microplate reader (Thermo, Varioskan Flash) was used to measure the absorption of each solution.

In Vitro and In Vivo Dual Modal Imaging

In vitro and in vivo dual modal imaging was performed on the microSPECT/CT scanner (Milabs, Utrecht, the Netherlands) with a multipinhole focused collimator. The SPECT was performed for 15 min per scan with energy window from 20 to 40 keV. Parameter of the CT scan was set as an accurate mode using three frames averaging, full angle, with 55 kV tube voltage, and 615 mA tube current. To evaluate the in vitro performance of dual modal imaging, concentrations of ^{125}I-PS varied from 0, 6.25, 12.5, 18.75 to 25 mg/mL, which corresponded to radioactivity of 0, 6.25, 12.5, 18.75 and 25 μCi, respectively, in tube phantom.

All animal experiments were operated following a protocol approved by the Animal Care and Use Committee of Soochow University. Female BALB/c mice (6 weeks of age, 20−23 g per animal) of specific pathogen free (SPF) grade were received from Shanghai SLAC Laboratory Animal Co., Ltd. The breast tumor model was established by subcutaneous injection of 4T1 cell suspension (~5×10^6 cells) into the flank region of the right back of mice and the consequent tumor was allowed to grow for 10 days. 4T1 tumor bearing mice were injected with ^{125}I-PS (1000 mg/kg, 200 μCi) by intravenous injection though the tail vein without thyroid pre-blocking. 1.5 % isoflurane/oxygen gas mixtures (flow rate: 0.6 L/min) were used to anesthetize the mice by inhalation on the temperature-controlled animal bed of the microSPECT/CT, scanned with varied times (0, 4, 6, 8, 12, 24 and 48 h). To study the retention of ^{125}I-PS in tumor, the acquisition times of 4T1 tumor bearing mice were scanned at

2, 6, 10, 14, 24, 48, 72, 96, 144 and 192 h post injection. All microSPECT/CT data were handled with POMD (Version 3.602) software.

Blood Circulation and Biodistribution

For in vivo pharmacokinetic studies, blood samples were collected from the retinal veins of healthy BALB/c mice (n=3) after post injection of ^{125}I-PS at 0, 1, 2, 4, 6, 8, 24 and 48 h, respectively. The blood samples were weighed and the radioactivity was measured by γ-counter (LB 2111 Multi Crystal Gamma Counter). To study biodistribution of ^{125}I-PS, major organs (heart, kidneys, liver, lungs and spleen) were weighed and radioactivity was measured.

In Vivo Therapy

4T1 tumor bearing BALB/c mice (30~50 mm^3) were randomly divided into two groups: I-PS and ^{131}I-PS (200 μCi, 50 mg/kg). The above agents were intravenously injected every 4 days at day 0, 4, 8, and 12 without thyroid pre-blocking. The tumor volume was monitored by a caliper every 2 days, and calculated according to the following equation: $V = LW^2/2$, where L and W are the length and width of the tumor, respectively. Data of body weight and death rate were recorded to evaluate the treatment performance. The relative tumor volume was calculated by V/V_0, where V_0 means the tumor volume on day 0. For histological analysis staining, tumor and major organs were harvested, fixed in 10 % neutral buffered formalin, embedded in paraffin. The tumor then was sectioned into thin slices and stained with hematoxylin and eosin (H&E).

Statistical analysis

All data were presented as the mean ± standard deviation (SD). One-way analysis of variance

(ANOVA) was used to assess significance between groups, after which post-hoc tests with the Bonferroni correction were used for comparison among individual groups. $^{*}p < 0.05$, was considered significant, and $^{**}p < 0.01$, $^{***}p < 0.001$ considered highly significant.

Results and Discussion

Preparation and Cytotoxicity of Radioactive Iodine-Rich Polymersomes

Iodine-rich polymer, PEG-PIC, was synthesized with an M_n of 5.0-50.0 kg mol^{-1}, which corresponded to an iodine content of 60.4 wt.%, according to our previous protocols.[48] PEG-PIC was radiolabeled with, radioisotopes, ^{125}I and ^{131}I, via isotopic exchange in dimethyl formamide (DMF) solution at 80 ^{o}C using acetate acid as a catalyst (Figure 1A). As shown in Figure 1B, ^{125}I radiolabeling efficiency increased with increasing time. The maximum radiolabeling yield was measured to be 63.9±6.3 % through thin layer chromatography (TLC) assay. The radiolabeling efficiency of ^{131}I-PS was similar to ^{125}I-PS (Figure S1). ^{125}I-labeled PEG-PIC readily formed polymersomes in water. Similar to non-radioactive I-PS, the dynamic size of ^{125}I-PS was 106 nm as determined by dynamic light scattering (DLS) assay (Figure 1C). Transmission electron microscopy (TEM) imaging showed that ^{125}I-PS had a spherical vesicular structure with an average size of 80 nm, which was close to the DLS data (Figure 1D). Hence, the isotopic exchange, with radioisotopes such as ^{125}I and ^{131}I has not changed the intrinsic properties of iodine-rich polymersomes. We further tested the radio stability of ^{125}I-PS and ^{131}I-PS in PBS and 10 % serum. The results showed little loss of ^{125}I and ^{131}I in 48 h (Figures S2 and S3), confirming a high radio stability. This radiolabeling strategy is easy, fast and stable.

Prior to the in vivo evaluation, we firstly investigated the potential cytotoxicity of I-PS, ^{125}I-PS and ^{131}I-PS in murine 4T1 breast cancer cells by the methyl thiazolyl tetrazolium (MTT) assay. No obvious toxicity to the 4T1 cells was observed even at a concentration of 5

mg/mL for I-PS. Notably, similar to non-radioactive I-PS, ^{125}I-PS was practically nontoxic to 4T1 cells even at a high concentration of 5 mg/mL, which corresponded to a radioactivity of 12 μCi (Figure 1E), suggesting that ^{125}I-PS has good safety. The lack of cytotoxicity of ^{125}I-PS is likely due to its low dose, as ^{125}I causes DNA strand break via Auger electron that works only when close to the cell nucleus. With ^{125}I both high dose and nuclear entry are required for effective radiotherapy. However, ^{131}I-PS caused obvious toxicity to 4T1 cells due to the released β rays from the ^{131}I. The immunofluorescence cell experiments further confirmed that ^{131}I-PS caused the DNA double strand breaks while I-PS and ^{125}I-PS did not (Figure S4). Therefore, ^{125}I labeled I-PS might be used for SPECT/CT imaging of mice bearing 4T1 tumors, while ^{131}I labeled I-PS might act as therapeutic agents for radioisotope therapy of tumor.

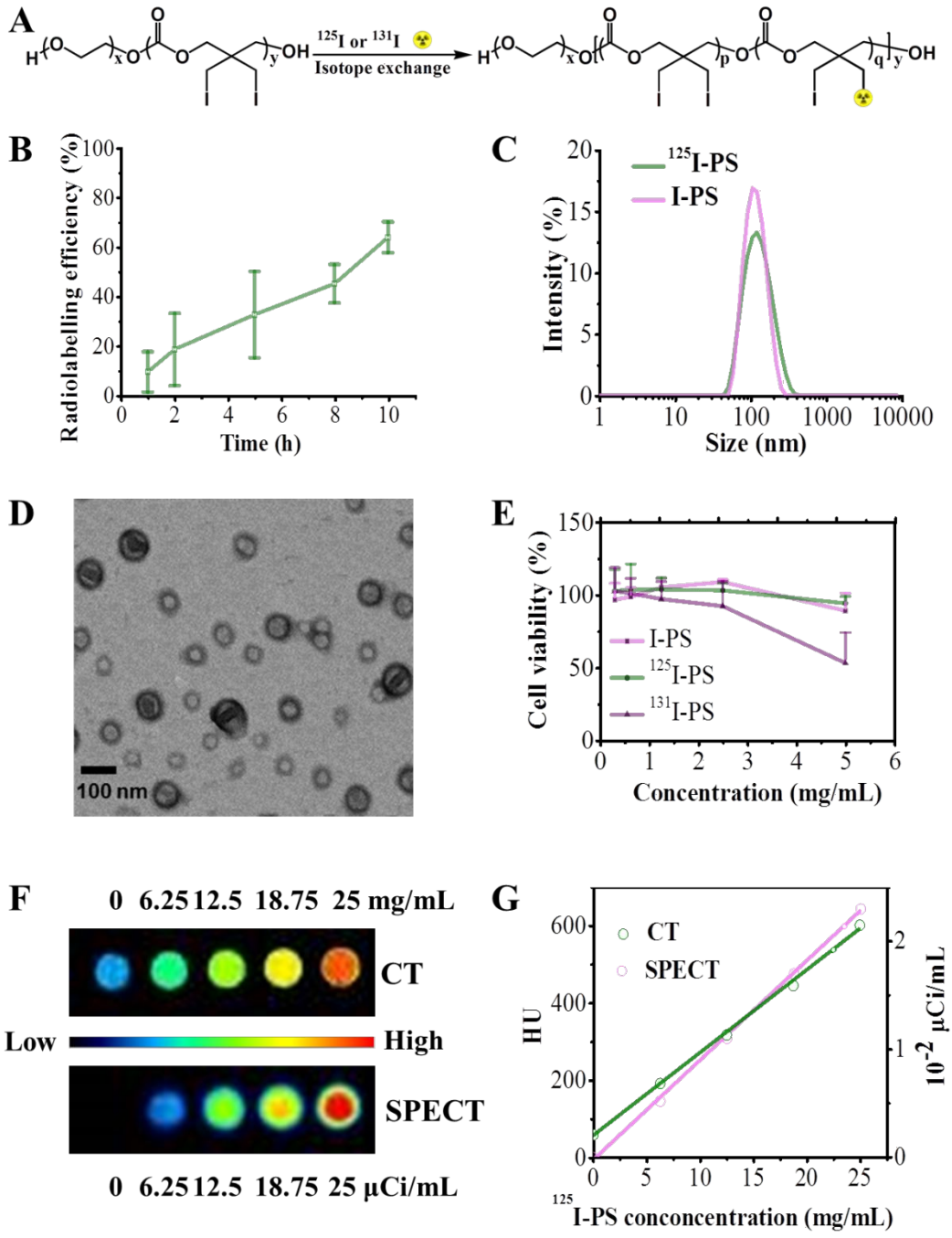

Figure 1. Synthesis and characterization of radiolabeled polymersomes: (A) Synthesis of PEG-PIC(^{125}I) and PEG-PIC(^{131}I) by isotopic exchange. (B) Radiolabeling efficiency as a function of time. The iodine exchange reaction was carried out with 200 μCi Na^{125}I in DMSO at 80 ˚C. (C) Size distribution profiles of I-PS and ^{125}I-PS measured by DLS. (D) TEM image of ^{125}I-PS. (E) MTT assays of I-PS, ^{125}I-PS and ^{131}I-PS at polymer concentrations varying from 0.31 to 5 mg/mL in 4T1 cells following 48 h incubation (n=6) (corresponding ^{125}I-PS

and ^{131}I-PS radioactivity varying from 0.75 to 12 μCi). (F) Phantoms reconstructions of ^{125}I-PS measured at polymer concentrations varying from 1 to 25 mg/mL (corresponding radioactivity varying from 0 to 25 μCi). (G) Quantification of CT and SPECT from phantoms reconstructions.

In Vitro and In Vivo SPECT/CT Dual Modal Imaging

In our previous work, I-PS with a remarkably high iodine content of 60.4 wt.% has demonstrated to be an excellent CT contrast agent compared with the commercial contrast agent Iohexol.[48] To explore the potential of ^{125}I-PS for dual modal imaging, we performed in vitro SPECT/CT scan by using tube phantoms. It was found that the intensity of reconstructed images of both CT and SPECT increased by increasing the concentration of I-PS and ^{125}I radioactivity, respectively. The CT and SPECT images matched well with each other (Figure 1F). The quantitative analysis showed that X-rays attenuation value increased from 192.4 HU to 602 HU with increasing concentrations of ^{125}I from 6.25 to 25 mg/mL, owing to the large attenuation of X-rays by iodine atom.[43-46] The radioactivity intensity of ^{125}I-PS increased linearly from 0.52 x 10^{-2} to 2.3 x 10^{-2} μCi /mL from the SPECT imaging assay (Figure 1G). The phantom studies suggested that the developed ^{125}I-PS could be used for SPECT and CT dual modal imaging.

To study the in vivo performance of ^{125}I-PS, SPECT and CT dual modal imaging of ^{125}I-PS in mice bearing 4T1 tumor was conducted. The 3D images of SPECT showed that ^{125}I-PS exhibited whole body distribution after injection. After 48 h of injection, ^{125}I-PS showed high tumor accumulation (Figure 2A). Notably, ^{125}I-PS showed also a high accumulation in liver and spleen. By installing a tumor-targeting ligand such as antibody and peptide on ^{125}I-PS, we might reduce its accumulation in liver and spleen and further increase its tumor accumulation. On the other hand, no any radioactivity signal in thyroid of mice with ^{125}I-PS treatment was

detected, further demonstrating the excellent stability of our ^{125}I-PS in vivo. Notably, SPECT imaging only detects the radioisotope. We performed the CT imaging to locate the nanoparticles. As expected, CT imaging of mice also showed a high tumor accumulation after 48 h of injection. The CT imaging was in good accordance with the SPECT imaging (Figure 2B). The X-rays attenuation value of the tumor increased from 66 ± 3 HU at 0 h to 256 ± 3 HU at 48 h post injection (Figure 2C). Compared to currently used small molecular contrast agents, ^{125}I-PS provides a significantly longer detection window. Interestingly, quantitative SPECT measurements showed that the radioactivity intensity of tumor tissue increased from 2 ± 0.45 % ID g^{-1} (percentage of injected dose per gram of tissue) at 0.5 h post injection up to 17.45 ± 0.08 % ID g^{-1} at 48 h post injection (Figure 2D), confirming that I-PS can target to 4T1. The high tumor accumulation of ^{125}I-PS is likely due to a high vascularization of 4T1 tumor as well as, good stability and long circulation time of ^{125}I-PS, both critical to observed EPR effect.[52-54] The above results demonstrate that ^{125}I-PS can be used as a contrast agent for dual modal imaging. Of note, it is a practical challenge to balance the dose for dual-modal imaging due to difference in sensitivity. Here, I-PS can uniquely meet the dose requirements for SPECT and CT dual-modal imaging in that we can tailor ^{125}I-PS radioactivity to make it suitable for both SPECT and CT imaging.

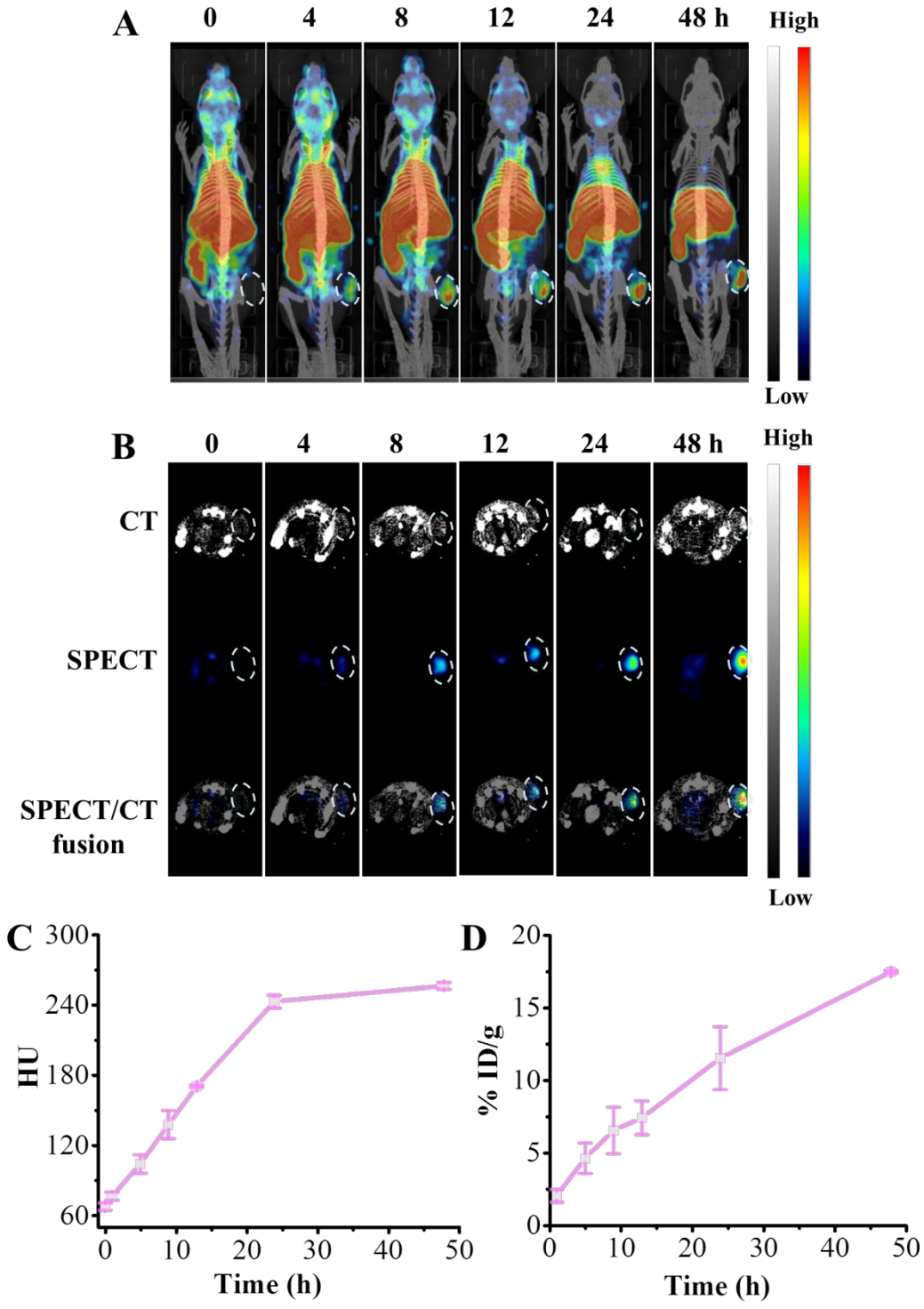

Figure 2. In vivo microSPECT/CT dual modal imaging of 4T1 tumor-bearing BALB/c mice at 0, 4, 8, 12, 24 and 48 h post injection of ^{125}I-PS. (A) 3D images of mice (4T1 tumor xenograft at right back-leg). (B) Coronal section of CT, SPECT and fusion images of mice (tumors marked with dashed circles). Tumor uptake quantified by CT (C) and SPECT (D).

Pharmacokinetic and Biodistribution

In order to study the in vivo behaviors of nanoparticles, healthy mice were intravenously injected with ^{125}I-PS without thyroid pre-blocking. After different time points, blood sample was collected from the retinal vein for radioactivity assay by gamma counter. The results showed that ^{125}I-PS exhibited long blood circulation time with pharmacokinetics followed a two-compartment model with the first and second phase blood circulation half-lives calculated to be 0.88 h ($t_{1/2\alpha}$) and 10.5 h ($t_{1/2\beta}$), respectively (Figure 3A). In contrast, free Na^{125}I showed significant accumulation in the thyroid and was rapidly cleared from the systemic circulation through kidney after intravenous injection (Figure S5).

We further studied the biodistribution of ^{125}I-PS in 4T1 tumor bearing mice. The tumor and major organs were excised at 48 h post intravenous injection of ^{125}I-PS (1000 mg/kg, 200 μCi) via tail vein. The radioactivity assays confirmed a high tumor accumulation of ^{125}I-PS (17.4 ± 0.1 % ID g^{-1}), which was significantly higher than that in the healthy organs such as heart, liver, lung, and kidney, except for spleen (Figure 3B). Figure S6 shows that ^{125}I-PS could be slowly excreted from the body with time. ^{125}I-PS is most likely degraded by enzymatic pathway in vivo, as reported for poly(trimethylene carbonate) and copolymers.[55, 56] The long circulation and favorable biodistribution make I-PS an interesting nanosystem for radioisotope therapy.

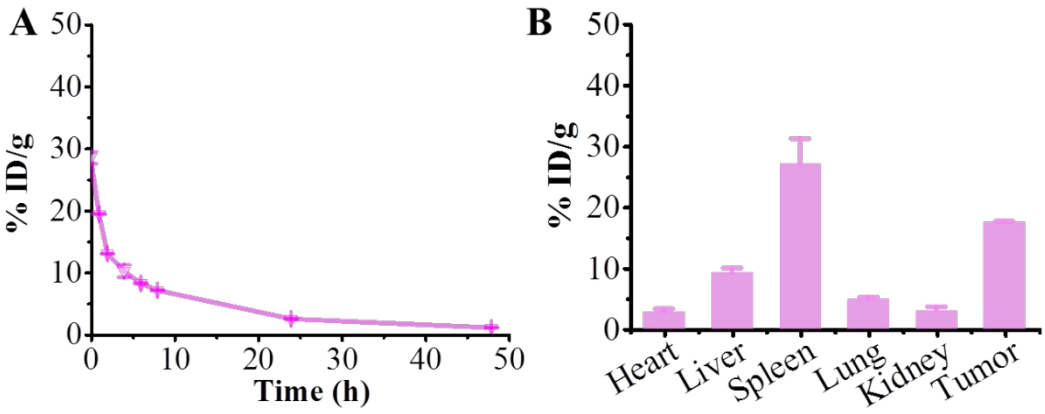

Figure 3. (A) The pharmacokinetics of ^{125}I-PS in mice following i.v. injection (n=3). (B) The

biodistribution of ^{125}I-PS in 4T1 tumor bearing BALB/c mice at 48 h post injection (n=3).

In Vivo Therapy

In order to assess the frequency of administration, we firstly monitored ^{125}I-PS in vivo for several days. As shown in Figure 4, tumor uptake of ^{125}I-PS reached a plateau on day 4 after injection. Combined with the half-life of ^{131}I, tumor uptake of ^{131}I-PS would reach the maximum on day 4 and then decrease. Under the guidance of SPECT/CT dual modal imaging, in vivo radioisotope therapy was conducted. Mice bearing 4T1 tumors were randomly divided into two group (n=5): I-PS and ^{131}I-PS. ^{131}I-PS was intravenously injected into mice every 4 days with radioactivity of 200 μCi and total four injections (given at day 0, 4, 8 and 12). Notably, ^{131}I-PS significantly inhibited tumor growth compared with the radio-inactive I-PS control (Figure 5A). Moreover, Kaplan-Meier survival curves showed that the mice treated with ^{131}I-PS had significantly longer median survival time than control group (32 versus 14 days) (Figure 5B). Meanwhile, ^{131}I-PS did not induce much loss of body weight compared with I-PS, demonstrating that ^{131}I-PS does not cause significant side effects (Figure 5C). Histological assays further revealed the tumor tissues from ^{131}I-PS treated mice exhibited remarkable cell necrosis while I-PS induced no obvious toxicity to cancer cells (Figure 5D). It should be further noted that little damage was observed in the normal tissues of ^{131}I-PS treated mice, further suggesting that ^{131}I-PS possesses good safety (Figure S7). Therefore, iodine-rich polymersomes enable not only SPECT/CT dual modal imaging but also potent radioisotope therapy of breast cancer in vivo.

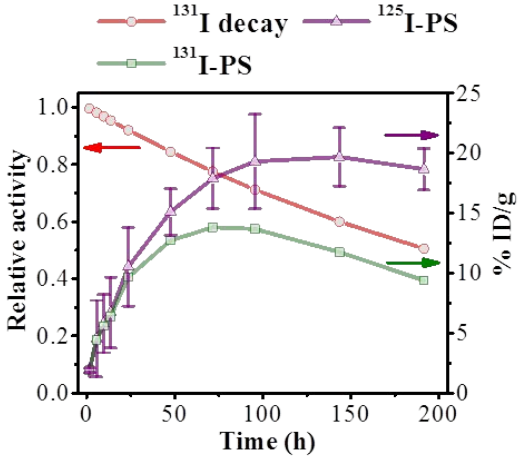

Figure 4. Tumor uptake of ^{131}I-PS predicted by ^{125}I-PS.

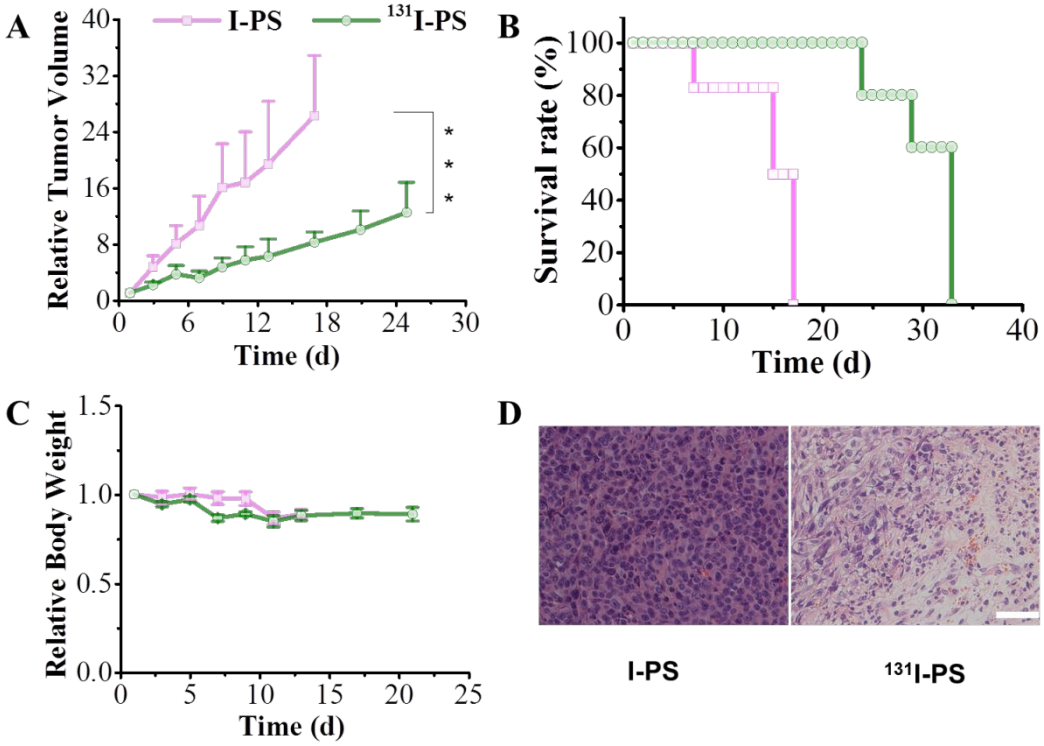

Figure 5. In vivo antitumor performance of ^{131}I-PS in 4T1 tumor-bearing mice. ^{131}I-PS was given on day 0, 4, 8 and 12 at radioactivity of 200 μCi. (n=5) (A) 4T1 tumor growth rate. Statistical analysis: One-way ANOVA with Tukey multiple comparison tests, $^{***}p<0.001$. (B) Survival curves of mice within 32 d. (C) Body weight changes of mice. (D) Macroscopic images of H&E stained sections of tumors excised on day 2. The scale bar corresponds to 100 μm.

Conclusion

We have demonstrated that iodine-rich-polymersomes (I-PS) can be used for SPECT/CT dual modal imaging as well as radioisotope therapy for 4T1 murine breast cancer in BALB/c mice. Interestingly, I-PS with high-efficiency and stable radiolabeling with ^{125}I or ^{131}I shows similar biophysical properties to the parent I-PS. As for I-PS, ^{125}I-PS is nontoxic, while ^{131}I-PS shows pronounced toxicity to 4T1 breast cancer cells. ^{125}I-PS provides effective and simultaneous contrast enhancement in tumor in vivo in both SPECT and CT imaging with a remarkable tumor accumulation of 17.45±0.08 % ID g^{-1} observed at 48 h post injection. The therapeutic studies clearly show that ^{131}I-PS effectively inhibits tumor growth without inducing obvious side effect. These iodine-rich polymersomes enabling SPECT/CT dual modal imaging and radioisotope therapy provide a novel and unique platform for cancer theranostics.

ASSOCIATED CONTENT

Supporting Information

The Supporting Information is available free of charge on the ACS Publications website. Experimental on immunofluorescence cell experiment; radiolabeling efficiency as a function of time, radio stability of ^{125}I-PS and ^{131}I-PS, DNA damage analysis of 4T1 cells following treatment with I-PS, ^{125}I-PS or ^{131}I-PS; 3D images of 4T1 tumor-bearing mice of Na(^{125}I) and ^{125}I-PS, and H&E stain sections of major organs.

AUTHOR INFORMATION

Corresponding author:

E-mail: glwang@suda.edu.cn; Tel: +86-512-65880054

E-mail: zyzhong@suda.edu.cn; Tel: +86-512-65880098

Notes

The authors declare no competing financial interest.

Acknowledgements

This work was supported by the National Key Research Program of China (2016YFC0101200), the National Natural Science Foundation of China (51603139, 81720108024), the Natural Science Foundation of Jiangsu Province (BK20160307), the Natural Science Foundation of Anhui Province (1508085SME220), the China Postdoctoral Science Foundation (2016M591915, 2018T110547) and Suzhou Administration of Science & Technology (SYS201701).

References

1. Weissleder R. Molecular Imaging in Cancer. *Science* **2006**, *312*,1168-1171.
2. Weissleder R.; Pittet M. Imaging in the Era of Molecular Oncology. *Nature* **2008**, *452*, 580-589.
3. Singh R.; Patel K.; Leong K.; Kim H. Progress in Nanotheranostics Based on Mesoporous Silica Nanomaterial Platform. *ACS Appl. Mater. Interfaces* **2017**, *9*, 10309-10337.
4. Lusic H.; Grinstaff M. X-ray-computed Tomography Contrast Agents. *Chem. Rev*. **2013**, *113*, 1641-1666.
5. Li X.; Anton N.; Zuber G.; Vandamme T. Contrast Agents for Preclinical Targeted X-ray Imaging, *Adv. Drug. Del. Rev*. **2014**, *76*, 116-133.
6. Lee S.; Jeon S.; Jung S.; Chun I.; Ahn C. Targeted Multimodal Imaging Modalities, *Adv. Drug. Del. Rev*. **2014**, *76*, 60-78.
7. Wang S.; Lin J.; Wang Z.; Zhou Z.; Bai R.; Lu N.; Liu Y.; Fu X.; Jacobson O.; Fan W.;

Qu J.; Chen S.; Huang P.; Chen X. Core-satellite Polydopamine Gadolinium Metallofullenren Nanotheranostics for Multimodal Imaging Guided Combination Cancer Therapy. *Adv. Mater*. **2017**, *29*, 1701013.

8. Cheng K.; Chen H.; Jenkins C.; Zhang G.; Zhao W.; Zhang Z.; Han F.; Fung J.; Yang M.; Jiang Y.; Xing L.; Cheng Z. Synthesis, Characterization, and Biomedical Applications of a Targeted Dual-modal Near-infrared-II Fluorescence and Photoacoustic Imaging Nanoprobe. *ACS Nano* **2017**, *11*, 12276-12291.
9. Yu B.; Wei H.; He Q.; Ferreira C.; Kutyreff C.; Ni D.; Rosenkrans Z.; Cheng L.; Yu F.; Egnle J.; Lan X.; Cai W. Efficient Uptake of ^{177}Lu-phorphyrin-PEG Nanocomplexes by Tumor Mitochondria for Multimodal-imaging Guided Combination Therapy. *Angew. Chem. Int. Ed*. **2018**, *57*, 218-222.
10. Tang J.; Zhou H.; Liu J.; Liu J.; Li W.; Wang Y.; Hu F.; Huo Q.; Li J.; Liu Y.; Chen C. Dual-mode Imaging-guided Synergistic Chemo- and Magnetohyperthermia Therapy in a Versatile Nanoplatform to Eliminate Cancer Stem Cells. *ACS Appl. Mater. Interfaces* **2017**, *9*, 23497-23507.
11. Zhou B.; Wang R.; Chen F.; Zhao L.; Wang P.; Li X.; Banyai I.; Ouyang Q.; Shi X.; Shen M. ^{99m}Tc-labeled RGD-polyethylenimine Conjugates with Entrapped Gold Nanoparticles in the Cavities for Dual-mode SPECT/CT Imaging of Hepatic Carcinoma. *ACS Appl. Mater. Interfaces* **2018**, *10*, 6146-6154.
12. Xu X.; Zhao L.; Li X.; Wang P.; Zhao J.; Shi X.; Shen M. Targeted Tumor SPECT/CT Dual Mode Imaging Using Multifunctional RGD-modified Low Generation Dendrimer-entrapped Gold Nanoparticles. *Biomater. Sci.* **2017**, *5*, 2393-2397.
13. Wen S.; Zhao L.; Zhao Q.; Li D.; Liu C.; Yu Z.; Shen M.; Majoral J.; Mignani S.; Zhao J.; Shi X. A Promising Dual Mode SPECT/CT Imaging Platform Based on ^{99m}Tc-labeled Multifunctional Dendrimer Entrapped Gold Nanoparticles. *J. Mater. Chem. B*. **2017**, *5*,

3810-3815.

14. Li X.; Xiong Z.; Xu X.; Luo Y.; Peng C.; Shen M.; Shi X. ^{99m}Tc-labeled Multifunctional Low-generation Dendrimer-entrapped Glod Nanoparticles for Targeted SPECT/CT Dual-mode Imaging of Tumors. *ACS Appl. Mater. Interfaces*. **2016**, *8*, 19883-19891.
15. Criscione J.; Dobrucki L.; Zhuang Z.; Papademetris X.; Simons M.; Sinusas A.; Fahmy T. Development and Application of a Multimodal Contrast Agent for SPECT/CT Hybrid Imaging. *Bioconjugate Chem.* **2011**, *22*, 1784-1792.
16. Wu Y.; Sun Y.; Zhu X.; Liu Q.; Cao T.; Peng J.; Yang Y.; Feng W.; Li F. Lanthanide-based Nanocrystals as Dual Modal Probes for SPECT and X-ray CT imaging. *Biomaterials* **2014**, *35*, 4699-4705.
17. Sun Y.; Zhu X.; Peng J.; Li F. Core-shell Lanthanide Upconversion Nanoparhosphors as Four-modal Probes for Tumor Angiogenesis Imaging. *ACS Nano* **2013**, 7, 11290-11300.
18. Chen G.; Roy I.; Yang C.; Prasad P. Nanochemistry and Nanomedicine for Nanoparticle-based Diagnostic and Therapy. *Chem. Rev.* **2016**, *116*, 2826-2885.
19. Smith B.; Gambhir S. Nanomaterials for In Vivo Imaging. *Chem. Rev*. **2017**, *117*, 901-986.
20. Muthu M.; Leong D.; Mei L.; Feng S. Nanotheranostics-Application and Further Development of Nanomedicine Strategies for Advanced Theranostics. *Theranostics* **2014**, *4*, 660-677.
21. Luk B.; Zhang L. Current Advances in Polymer-based Nanotheranostics for Cancer Treatment and Diagnosis. *ACS Appl. Mater. Interfaces* **2014**, *6*, 21859-21873.
22. Jo S.; Ku S.; Won Y.; Kim S.; Kwon I. Targeted Nanotheranostics for Future Personalized Medicine: Recent Progress in Cancer Therapy. *Theranostics* **2016**, *6*, 1362-1377.
23. Fan W.; Yung B.; Huang P. Nanotechnology for Multimodal Synergistic Cancer Therapy.

Chem. Rev. **2017**, *117*, 13566-13568.

24. Song L.; Zhao N.; Xu F. Hydroxyl-rich Polycation Brushed Multifunctional Rare-earth-gold Core Shell Nanorods for Versatile Therapy Platforms. *Adv. Funct. Mater.* **2017**, *27*, 1701255.
25. Palivan C.; Goers R.; Najer A.; Zhang X.; Car A.; Mejer W. Bioinspired Polymer Vesicles and Membranes for Biological and Medical Applications. *Chem. Soc. Rev*. **2016**, *45*, 377-411.
26. Leong J, Teo J.; Aakalu V.; Yang Y.; Kong H. Engineering Polymersomes for Diagnostics and Therapy. *Adv. Healthcare. Mater.* **2018**, 1701276.
27. Lee J.; Feijen J. Polymersomes for Drug Delivery: Design, Formation and Characterization. *J. Control. Release*. **2012**, *161*, 473-483.
28. Kamaly N.; Xiao Z.; Valencia P.; Radovic-Moreno A.; Farokhzad O. Targeted Polymeric Therapeutic Nanoparticles: Design, Development and Clinical Translation. *Chem. Soc. Rev.* **2012**, *41*, 2971-3010.
29. Wang F.; Xiao J.; Chen S.; Sun H.; Yang B.; Jiang J.; Zhou X.; Du J. Polymer Vesicles: Modular Platforms for Cancer Theranostics. *Adv. Mater.* **2018**, *30*,17056674.
30. Pant K.; Sedlacek O.; Nadar R.; Hruby M.; Stephan H. Radiolabelled Polymeric Materials for Imaging and Treatment of Cancer: Quo Vadis? *Adv. Healthcare. Mater.* **2017**, 1601115.
31. Elsabahy M.; Heo G.; Lim S.; Sun G.; Wooley K. Polymeric Nanostructures for Imaging and Therapy. *Chem. Rev.* **2015**, *115*, 10967-11011.
32. Zhang N.; Chen H.; Fan Y.; Zhou L.; Trepout S.; Guo J.; Li M. Fluorescent Polymersomes with Aggregation-induced Emission. *ACS Nano* **2018**, *12*, 4025-4025.
33. Yang K.; Liu Y.; Liu Y.; Zhang Q.; Kong C.; Yi C.; Zhou Z.; Wang Z.; Zhang G.; Zhang Y.; Khashab N.; Chen X.; Nie Z. Cooperative Assembly of Magneto-nanovesicles with

Tunable Wall Thickness and Permeability for MRI-Guided Drug Delivery. *J. Am. Chem. Soc.* **2018**, *140*, 4666-4677.

34. Oliveira H.; Perez-Andres E.; Thevenot J.; Sandre O.; Berra E.; Lecommandoux S. Magnetic Field Triggered Drug Release from Polymersomes for Cancer Therapeutics. *J. Control. Release.* **2013**, *169*, 165-170.
35. Liu J.; Song L.; Chen S.; Gao J.; Zhao P.; Du J. A Superparamagnetic Polymersome with Extremely High T2 Relaxivity for MRI and Cancer Targeted Drug Delivery. *Biomaterials* **2017**, *114*, 23-33.
36. Liu G.; Liu X.; Wang S. Biomimetic Polymersomes as Carriers for Hydrophilic Quantum Dots. *Langmuir* **2012**, *28*, 557-562.
37. Brinkhuis R.; Stojanov K.; Laverman P.; Eilander J.; Zuhorn I.; Rutjes F.; van Hest J. Size Dependent Biodistribution and SPECT Imaging of ^{111}In-Labeled Polymersomes. Bioconjuate Chem. 2012, *23*, 958-965.
38. Wang G.; Kruijff R.; Stuart M.; Mendes E.; Wolterbeek T.; Denkova A. Polymersomes as Radionuclide Carriers Loaded via Active Ion Transport Through the Hydrophobic Bilayer. *Soft Matter* **2013**, *9*, 727-734.
39. Hu X.; Zhai S.; Liu G.; Xing D.; Liang H.; Liu S. Concurrent Drug Unplugging and Permeabilization of Polyprodrug-gated Crosslinked Vesicles for Cancer Combination Chemotherapy. *Adv. Mater.* **2018**, *30*, 1706307.
40. Zhang Y.; Wu K.; Sun H.; Zhang J.; Yuan J.; Zhong Z. Hyaluronic Acid-shelled Disulfide-cross-linked Nanopolymersomes for Ultrahigh-efficiency Reactive Encapsulation and CD44-targeted Delivery of Mertansine Toxin. *ACS Appl. Mater. Interfaces* **2018**, *10*, 1597-1604.
41. Jiang Y.; Zhang J.; Meng F.; Zhong Z. Apolipoprotein E Peptide-directed Chimeric Polymersomes Mediate an Ultrahigh-efficiency Targeted Protein Therapy for

Glioblastoma. *ACS Nano* **2018**, *12*, 11070-11079.

42. Shi Y.; Jiang Y.; Cao J.; Yang W.; Zhang J.; Meng F.; Zhong Z. Boosting RNAi Therapy for Orthotopic Glioblastoma with Nontoxic Brain-targeting Chimaeric Polymersomes. *J. Control. Release.* **2018**, *292*, 163-171.
43. You S.; Jung H.; Lee C.; Choe Y.; Heo J.; Gang G.; Byun S.; Kim W.; Lee C.; Kim D.; Kim Y.; Kim Y. High-performance Dendritic Contrast Agents for X-ray Computed Tomography Imaging Using Potent Tetraiodobenzen Derivatives. *J. Controll. Release.* **2016**, *226*, 258-267.
44. Attia M.; Anton N.; Chiper M.; Akasov R.; Anton H.; Messaddeq N.; Fournel S.; Klymchenko A.; Mely Y.; Vandamme T. Biodistribution of X-ray Iodinated Contrast Agent in Nano-emulsion is Controlled by the Chemical Nature of the Oily Core. *ACSNano* **2014**, *8*, 10537-10550.
45. Sun Y.; Hu H.; Yu B.; Xu F. PGMA-based Cationic Nanoparticles with Polyhydric Iodine Units for Advanced Gene Vectors. *Biconjugate. Chem.* **2016**, *27*, 2744-2754.
46. Yin Q.; Yap F.; Yin L.; Ma L.; Zhou Q.; Dobrucki L.; Fan T.; Gaba R.; Cheng J. Poly(iohexol) Nanoparticles as Contrasts Agents for In Vivo X-ray Computed Tomography Imaging. *J. Am. Chem. Soc.* **2013**, *135*, 13620-13623.
47. Lee J.; Chung S.; Cho H.; Kim D. Iodinated Hyaluronic Acid Oligomer-based Nanoassemblies for Tumor-targeted Drug Delivery and Cancer Imaging. *Biomaterials* **2016**, *85*, 218-231.
48. Zou Y.; Wei Y.; Wang G.; Meng F.; Gao M.; Storm G.; Zhong Z. Iodine-Rich Nano-Polymersomes as a High-Performance X-Ray Computed Tomography Contrast Agent. *Adv. Mater.* **2017**, *29*, 1603997.
49. Zhao L.; Zhu J.; Cheng Y.; Xiong Z.; Tang Y.; Guo L.; Shi X.; Zhao J. Chlorotoxin-conjugated Multifunctional Dendrimers Labeled with Radionuclide ^{131}I for

Single Photon Emission Computed Tomography Imaging and Radiotherapy of Gliomas. *ACS Appl. Mater. Interfaces.* **2015**, *7*, 19798-19808.

50. Chen Y.; Zhu J.; Zhao L.; Xiong Z.; Tang Y.; Liu C.; Guo L.; Qiao W.; Shi X.; Zhao J. ^{131}I-labeled Multifunctional Dendrimers Modified with Bmk CT for Targeted SPECT Imaging and Radiotherapy of Giomas. *Nanomedicine* **2016**, *11*, 1253-1266.
51. Zhu J.; Zhao L.; Cheng Y.; Xiong Z.; Tang Y.; Shen M.; Zhao J.; Shi X. Radionuclide ^{131}I-labeled Multifunctional Dendrimers for Targeted SPECT Imaging and Radiotherapy of Tumors. *Nanoscale* **2015**, *7*, 18169.
52. Mei K.; Bai J.; Lorrio S.; Wang J.; AI-Jamal K. Investigating the Effect of Tumor Vascularization on Magnetic Targeting In Vivo Using Retrospective Design of Experiment. *Biomaterials* **2016**, *106*, 276-285.
53. Perry J.; Reuter K.; Luft J.; Pecot C.; Zamboni W.; DeSimone J. Mediating Passive Tumor Accumulation Through Particle Size, Tumor Type, and Location. *Nano Lett.* **2017**, *17*, 2879-2886.
54. Ojha T.; Pathak V.; Shi Y.; Hennink W.; Moonen C.; Strom G.; Keissling F.; Lammers T. Pharmacological and Physical Vessel Modulation Strategies to Improve EPR-mediated Drug Targeting to Tumors. *Adv. Drug. Deliv. Rev.* **2017**, *119*, 44-60.
55. Zhang Z.; Kuijer R.; Bulstra SK.; Grijpma D.; Feijen J. The In Vivo and In Vitro Degradation Behavior of Poly(trimethylene carbonate). *Biomaterials* **2006**, *27*, 1741-1748.
56. Yang L.; Li J.; Meng S.; Jin Y.; Zhang J.; Li M.; Guo J.; Gu Z. The In Vivo and In Vitro Degradation Behavior of Poly(trimethylene carbonate-co-ε-caprolactone) implants. *Polymer* **2014**, *55*, 5111-5124.

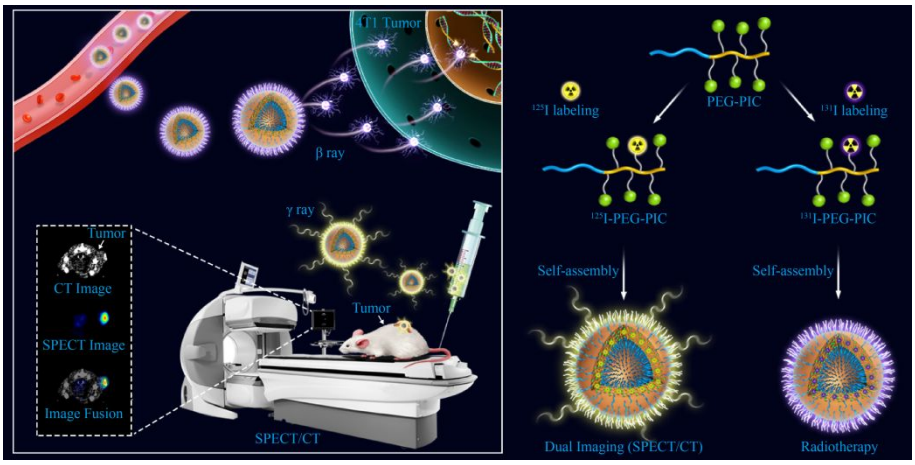

Table of Contents Graphic